Journal of Propulsion and Power
Vol. 35, No. 2, March–April 2019

Linear Acoustic Analysis of the Preburner of an Oxidizer-Rich Staged Combustion Engine

Christopher Lioi,* David Ku,† and Vigor Yang‡
Georgia Institute of Technology, Atlanta, Georgia 30327-0150

DOI: 10.2514/1.B37132

The linear acoustic behavior of an oxidizer-rich staged combustion engine preburner assembly that was similar to that of the RD-170 has been investigated by using real fluid speeds of sound to accommodate supercritical pressures. The speeds of sound, and hence the resulting frequencies, were approximately 20% higher than would be expected from ideal gas assumptions, which is a critical point of difference between the acoustic behavior of the preburner versus the main chamber. The results show that the mode shapes in the preburner–turbine inlet assembly are largely invariant with respect to the boundary condition used for the turbine blade row, but the frequencies are noticeably affected. The 2L mode is totally suppressed for both the acoustically open case and the case with the blade row impedance condition. The remaining longitudinal modes are damped. Both the frequency and the mode shape of the 1T mode remain totally invariant because the oscillations are confined to the injector regions and do not exhibit acoustic velocity with components normal to the impedance surface. The lack of damping of the 1T mode by the blade rows, combined with the relatively high magnitudes of acoustic velocity near the combustion zone, suggests that the 1T mode is a likely candidate to experience instability if it is suitably energized by the heat release.

Nomenclature

c	=	speed of sound
$\mathcal{D}$	=	acoustic dipole sources
$\mathcal{F}$	=	fluctuating interphase momentum transfer, due to phase change and drag forces
k	=	wave number; $\Omega/\bar{c}$
L	=	turbine blade chord length
$\mathcal{M}$	=	acoustic monopole sources
$\boldsymbol{n}$	=	inner unit normal vector of chamber wall
$\mathcal{P}$	=	fluctuating energy release due to combustion, work done by condensed phase, and energy transfer due to phase change
p	=	pressure
$\boldsymbol{u}$	=	velocity vector
Z	=	acoustic impedance; $p'/(\boldsymbol{u}'\cdot\boldsymbol{n})$
α	=	angle between incident wave and surface normal
γ	=	ratio of specific heats
θ	=	angle of attack of turbine blades
Ω	=	$\omega + i\alpha$; complex eigenfrequency, where ω is equal to the angular frequency of oscillation and α is equal to the damping rate

Superscripts

$-$	=	averaged quantity
$'$	=	fluctuating quantity
$\hat{}$	=	complex amplitude

I. Introduction

OXYGEN-RICH staged combustion (ORSC) engines have been widely used for space launch vehicles due to numerous thermodynamic advantages [1]. In a staged combustion cycle, a small fraction of fuel is burned in one or more preburners to drive the turbopump assembly. The resultant hot products of combustion are delivered into the thrust chamber along with the remainder of the fuel. As compared with expander or gas-generator cycle engines, the ORSC engine exhibits higher propulsive efficiency and thrust-to-weight ratio, as well as improved combustion stability characteristics. Furthermore, in the oxidizer-rich mode with hydrocarbon fuel, the engine experiences substantially less coking, with little carbon deposition on the turbine. This contributes to lower maintenance requirements and higher engine operational lifetime and reliability.

Like the main combustion chamber, however, the preburners in an ORSC engine are susceptible to combustion instabilities. Figures 1 and 2 show schematically a single preburner and two preburners feeding the inlet hub of the turbine, respectively, of a generic approximation to the RD-170 engine [2,3]. Figure 3 shows a cross-section of the preburner injector which is used in both configurations. The underlying physics of the instability problem are the same for the two geometries. Unsteady motions within the chamber perturb the flame, which causes a modulation of the rate of heat release. The resulting unsteady gas expansion drives acoustic oscillations that, in turn, perturb the flame, thereby establishing a feedback loop for sustaining instability. When more energy is added to the acoustic field than is radiated out of the chamber or dissipated internally, the oscillations grow until they reach a limiting amplitude [4].

Many different strategies have been used to analyze and predict the onset of combustion instabilities, with extensive research literature dedicated to liquid propellant rocket engines. Of particular interest to designers is the initial period of linear growth preceding the establishment of destructive limit-cycle oscillations. If the system is stable, ignoring exotic nonnormality effects [5,6], then small-amplitude disturbances should decay. Thus, it is advantageous to design a combustion chamber in which all modes of concern are linearly stable. Several prediction methodologies have been explored based on linearized conservation equations [7,8]. A linear stability analysis following the formulation of Culick and Yang [9] was developed in our previous study and applied to a main combustion chamber modeled on the RD-170 engine. The present work is a direct continuation of Ref. [10] and is focused on the linear acoustics of its preburner counterpart.

The preburners of an ORSC engine operate at significantly higher pressure and lower temperature than the main combustion chamber, and the thermodynamic states of the fluids involved are in the transcritical or supercritical regime [11]. Ideal gas behavior cannot be assumed, and a real fluid equation of state must be introduced to close the theoretical formulation. The typical extreme operating conditions

Received 9 March 2018; revision received 1 October 2018; accepted for publication 3 October 2018; published online 7 December 2018.

*Graduate Research Assistant, Aerospace Engineering; clioi3@gatech.edu. Student Member AIAA.

†Research Engineer, School of Aerospace Engineering; currently Research Engineer, Aerojet Rocketdyne, Sacramento, California; d.ku@gatech.edu. Member AIAA.

‡William R. T. Oakes Professor and Chair, School of Aerospace Engineering; vigor.yang@aerospace.gatech.edu. Fellow AIAA.

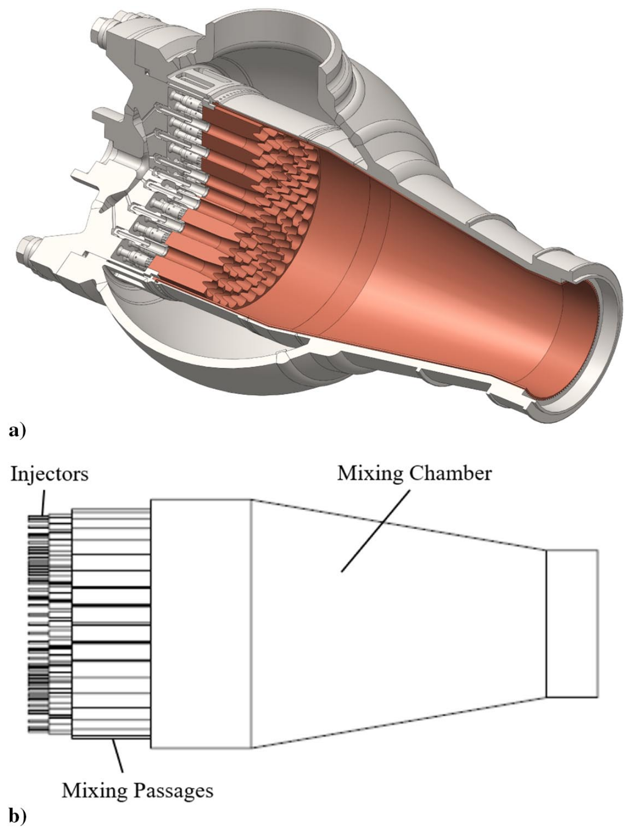

Fig. 1 Representations of a) ORSC engine preburner model and b) longitudinal cutaway. Adapted from the work of Yang et al. [2].

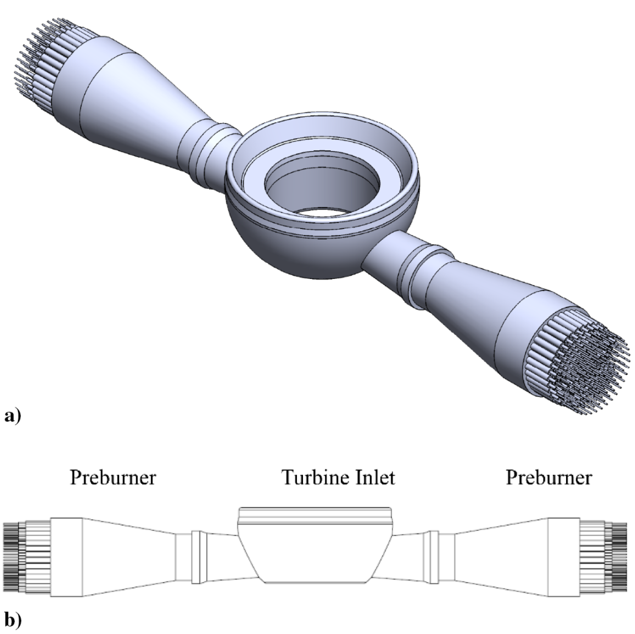

Fig. 2 ORSC engine preburner–turbine assembly: a) three-quarter view, and b) longitudinal cross section. Adapted from the work of Yang et al. [2].

pose severe challenges to experimental studies on the stability of candidate designs, and so it is imperative that effective stability prediction methodologies based on first principles be developed to mitigate the cost and risk of experimental validation.

As shown in Fig. 2b, the products of combustion from the preburners enter the turbine inlet hub and flow through an annular passage leading to the turbine blades. Because the model domain is truncated at this plane, the reflection of acoustic waves by the turbine blade rows must be quantified with an impedance boundary

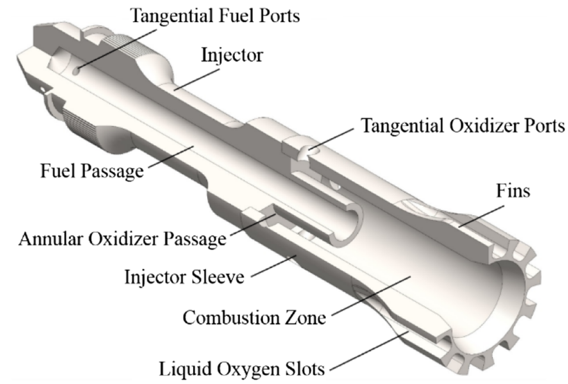

Fig. 3 Cross section of preburner injector [1,2].

condition. This problem was first addressed in the study by Kaji and Okazaki [12,13], in which the effects of the mean flow Mach number, blade spacing, and relative angle between the blades and the flow were quantified as a function of wave number. Muir [14] generalized the analysis to allow for a three-dimensional acoustic field and nontrivial blade camber. Backpropagating acoustic waves can also be generated due to the acceleration of nonisentropic density or temperature fluctuations (known collectively as entropy waves) as well as vorticity waves through the rotor–stator assembly [15]. Cumpsty and Marble [16] used a quasi-one-dimensional theory to determine the reflected pressure wave in such a scenario at low frequencies. Recently, high-fidelity techniques such as the large-eddy simulation (LES) have been employed to explore this mechanism from the perspective of combustion noise and elucidate in more detail the effect of blade geometry [17].

This paper is organized as follows. In Sec. II, the acoustic formulation is briefly reviewed, along with the evaluation of the real fluid speed of sound and the impedance boundary condition at the turbine inlet. Section III presents the eigenmode analysis for both a single preburner and a combined preburner–turbine configuration. The underlying physics for various boundary conditions are considered. Section IV concludes the work.

II. Methodology

A. Acoustic Wave Equation

The analysis follows the approach described in Ref. [10] for the main combustor; it is briefly reviewed here. The basis of the theoretical formulation is the acoustic wave equation derived from the conservation laws. The gas properties are assumed constant and uniform, and the fluid throughout the volume is assumed to consist of only a single phase. The latter assumption is justified because distinct liquid and gas phases cannot be identified at the supercritical pressure considered in this work [11]. Under these assumptions, the wave equation for the acoustic pressure can be written as

$$\frac{1}{\bar{\rho}\bar{c}^2}\frac{\partial^2 p'}{\partial t^2} - \frac{1}{\bar{\rho}}\nabla^2 p' = -\mathcal{M} + \frac{1}{\bar{\rho}}\nabla\cdot\boldsymbol{\mathcal{D}} \tag{1}$$

where the source terms have been collected into monopole sources given by

$$\mathcal{M} = \frac{1}{\bar{\rho}\bar{c}^2}\left(\bar{\boldsymbol{u}}\cdot\nabla\frac{\partial p'}{\partial t} + \frac{\partial(\boldsymbol{u}'\cdot\nabla p')}{\partial t} - \frac{\partial\mathcal{P}'}{\partial t} + \Gamma\right) \tag{2}$$

and dipole sources given by

$$\boldsymbol{\mathcal{D}} = \bar{\rho}(\bar{\boldsymbol{u}}\cdot\nabla\boldsymbol{u}' + \boldsymbol{u}'\cdot\nabla\bar{\boldsymbol{u}}) + \left(\bar{\rho}\boldsymbol{u}'\cdot\nabla\boldsymbol{u}' + \rho'\frac{\partial\boldsymbol{u}'}{\partial t}\right) - \boldsymbol{\mathcal{F}}' \tag{3}$$

In the preceding equations and throughout this paper, primes indicate fluctuating quantities and overbars indicate time-averaged quantities. On the right-hand side of Eq. (1), the source terms have been grouped into monopole-like and dipole-like contributions. The groups $\mathcal{P}'$ and $\boldsymbol{\mathcal{F}}'$ represent, respectively, the contributions from chemical heat release and volumetric forces, interphase momentum transfer, and surface forces. Group Γ contains terms that, under the ideal gas assumption, involve gradients of mean velocity with the ratio of specific heats $\bar{\gamma}$ as a coefficient, but which, at supercritical pressures, take a more complicated form due to the invocation of real fluid thermodynamic relationships. In the present work, we only consider nonreacting flows. Thus, both $\mathcal{P}'$ and $\boldsymbol{\mathcal{F}}'$ are set to zero.

We assume that all unsteady quantities vary harmonically in time as follows:

$$p' = \hat{p}e^{i\Omega t} \qquad \boldsymbol{u}' = \hat{\boldsymbol{u}}e^{i\Omega t} \tag{4}$$

where the overhat denotes a complex spatial amplitude. Here, Ω is the complex frequency defined as $\Omega = \omega + i\alpha$, with ω and α being the radian frequency and damping coefficient, respectively. With this sign convention, negative values of α indicates a wave growing in amplitude, whereas a positive value indicates a damped wave. Substituting Eq. (4) into Eq. (1) and neglecting all nonlinear terms, we have

$$-\frac{1}{\bar{\rho}}\left(\frac{\Omega^2}{\bar{c}^2}\hat{p} + \nabla^2\hat{p}\right) = -\frac{i\Omega}{\bar{\rho}\bar{c}^2}\bar{\boldsymbol{u}}\cdot\nabla\hat{p} + \nabla\cdot(\bar{\boldsymbol{u}}\cdot\nabla\hat{\boldsymbol{u}} + \hat{\boldsymbol{u}}\cdot\nabla\bar{\boldsymbol{u}}) \tag{5}$$

Finally, disregarding mean flow, we have the following:

$$-\frac{1}{\bar{\rho}}\left(\frac{\Omega^2}{\bar{c}^2}\hat{p} + \nabla^2\hat{p}\right) = 0 \tag{6}$$

subject to the impedance condition Z along the boundary

$$-\frac{1}{\bar{\rho}}(\boldsymbol{n}\cdot\nabla\hat{p}) = i\Omega\frac{\hat{p}}{Z} \tag{7}$$

The eigenvalue analysis of the preburner is conducted using Eqs. (6) and (7), in which the only remaining fluid parameters are the density and speed of sound. The eigenvalue problem is solved numerically using the commercial finite element code COMSOL for both the single preburner geometry and the preburner–turbine inlet hub assembly as shown in Figs. 1 and 2, respectively. Modal finite element matrices are built by the discretization of Eqs. (6) and (7) over the geometries shown after discretization by conforming tetrahedral meshes.

B. Real Fluid Properties

The preburner of concern (the RD-170 engine) uses RP-1 (Rocket-Propellant 1) kerosene as fuel and liquid oxygen as oxidizer. The kerosene fuel is a mixture of various hydrocarbons with an overall ratio of hydrogen to carbon atoms of 1.94. To simplify the chemical kinetics modeling, heptylcyclopentane ($C_{12}H_{24}$), which is a single-species surrogate fuel, is considered. Its thermodynamic properties closely approximate those of RP-1 [18]. The stoichiometric equation of this surrogate fuel with oxygen can be written as

$$C_{12}H_{24} + 18O_2 \rightarrow 12CO_2 + 12H_2O$$

Table 1 gives the operating condition of a generic RD-170 preburner.

The fluid thermodynamic properties in the preburner are required for accurate prediction of acoustic behaviors. Owing to the high pressure and relatively low temperature developed in the preburner, real fluid effects cannot be ignored. In a general fluid mixture, the speed of sound is computed by

$$\bar{c}^2 = \frac{c_p}{c_V}\left(\frac{\partial p}{\partial \rho}\right)_{T,Y_k} \tag{8}$$

where p and ρ are related by an appropriate real fluid equation of state [11,19]. Likewise, the constant-pressure and constant-volume specific heat capacities are computed for the given temperature from NASA polynomial fits. For the computations in this work, we use the National Institute of Standards and Technology's (NIST's) REFPROP code [20], which uses molecular data from the extensive NIST database and high-fidelity explicit equations of state based on the Helmholtz free energy [21]. This model is known to exhibit better agreement with experimental data than typical cubic equations of state for several elementary hydrocarbon species. Figure 4 shows a comparison between the calculated speeds of sound of the combustion products in the preburner and the corresponding values for an ideal gas at the same conditions.

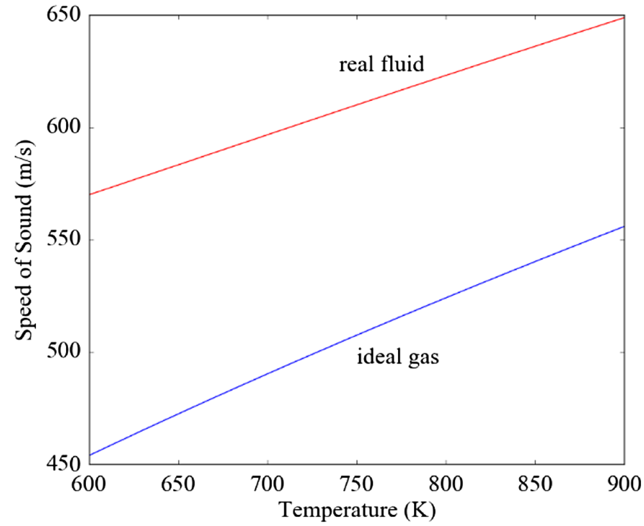

Fig. 4 Speeds of sound of ideal and real fluids for preburner combustion products at $\bar{p} = 52$ MPa and $\phi = 6.55 \times 10^{-2}$.

The real fluid speeds nearly mirror the $\sim\sqrt{T}$ temperature dependence of the ideal gas speed of sound. However, the reduction in compressibility due to intermolecular forces causes the speed of sound to be approximately 20% higher for the real fluid versus the ideal gas over the entire temperature range investigated. It should be noted that the chemical composition of the mixture for these calculations is chosen by assuming complete combustion without product dissociation. The former assumption is justified by the extremely oxidizer-rich environment in the preburner, and the latter is justified by the high chamber pressure.

Combustion is initiated in the injector passage. The wide mixing passages and the bulk of the chamber are where the combustion products mix with the cold unburned oxidizer, so as to allow the temperature and composition to become spatially uniform. The temperature in the injector passage is significantly higher than in the rest of the chamber. Table 2 lists the corresponding densities and speeds of sound populated in the model.

Table 1 Operating conditions of RD-170 preburner

Parameter	Value
O/F ratio	52.31
Equivalence ratio	6.55×10^{-2}
Main chamber pressure, MPa	52
Injection element temperature, K	2112
Mixing passage temperature, K	947.3
Main chamber temperature, K	785.5

Table 2 Fluid properties for each subdomain computed from REFPROP

	Injection element	Mixing passage	Main chamber
$\bar{\rho}$, kg/m	87.5	185	220
$\bar{c}$, m/s	903	660	619

C. Turbine Inlet Impedance

Figure 5 shows a schematic of the central turbopump shaft for the approximation to the RD-170 engine. In the present work, entropy waves are ignored and only an acoustic boundary condition is required. Because the turbine hub-to-tip length is small in comparison with the average turbine radius, we may employ the thin annulus approximation such that the turbine blade row may be conceptually unrolled and treated in a quasi-one-dimensional manner. Given these model stipulations, we may employ impedance values based on the semiactuator disk theory of Refs. [12–14]. Figure 6 shows nominally plane acoustic waves interacting with a blade row of chord length L and angle θ with respect to the horizontal.

The wave incident on the blade row at some angle α is partially reflected and transmitted. We express the pressure fields in the upstream p'_- and downstream p'_+ regions of the blade row as a superposition of plane waves as shown in Fig. 6:

$$p'_+(x,y,t) = p'_i(x,y,t) + \mathcal{R}p'_r(x,y,t) \tag{9}$$

$$p'_-(x,y,t) = \mathcal{T}p'_t(x,y,t) \tag{10}$$

where $\mathcal{R}$ and $\mathcal{T}$ denote the reflection and transmission coefficients, respectively. Matching the fields across the blade row by means of the linearized conservation equations yields expressions for the wave amplitudes. An equivalent impedance may be put in terms of the reflection coefficient as

$$\frac{Z}{\bar{\rho}\,\bar{c}} = \frac{1+\mathcal{R}}{1-\mathcal{R}}\frac{1}{\cos\alpha} \tag{11}$$

In the limit of the negligible mean flow Mach number, using the results from Ref. [12], we have

$$\frac{Z}{\bar{\rho}\,\bar{c}} = \frac{1}{\cos\alpha}\left[2\sqrt{1+\frac{\sin^2 kL}{4}\left(\frac{\cos\theta}{\cos\alpha}-\frac{\cos\alpha}{\cos\theta}\right)^2}-1\right] \tag{12}$$

Figure 7 shows example calculations for both the reflection coefficient and the impedance for a fixed blade angle of attack θ and several different angles of incidence α. For a nominal blade chord length of 0.08 m, the wave number covers a frequency range of 0–3870 Hz.

Equation (12) reveals some important special cases that are of interest to designers. For all angles of incidence, the reflection coefficient is maximized at $kL = \pi/2$ when the blade chord length is equal to one-quarter of the acoustic wavelength. Likewise, it vanishes at $kL = \pi$ when the blade chord length is equal to one-half of the acoustic wavelength because there is no phase difference between the incident and transmitted waves. The latter case presents an attractive

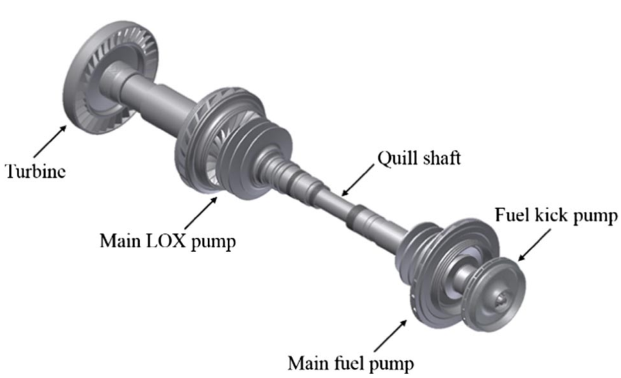

Fig. 5 General model of RD-170 turbopump rotor assembly. Adapted from Ref. [2].

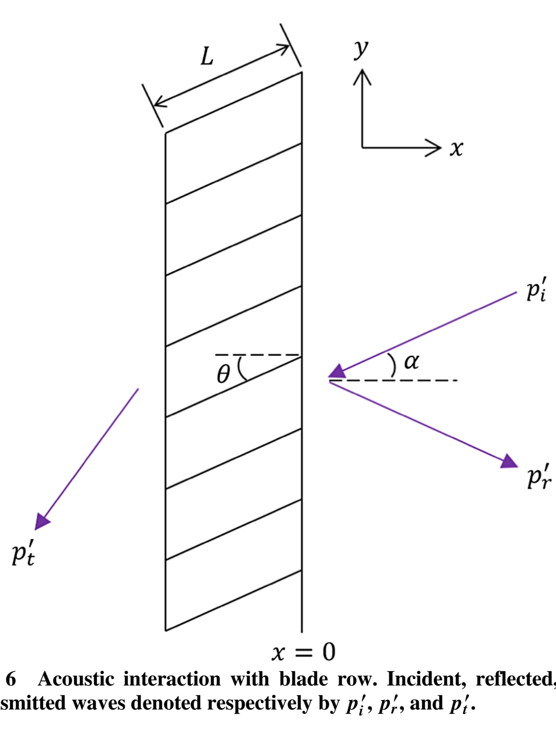

Fig. 6 Acoustic interaction with blade row. Incident, reflected, and transmitted waves denoted respectively by p'_i, p'_r, and p'_t.

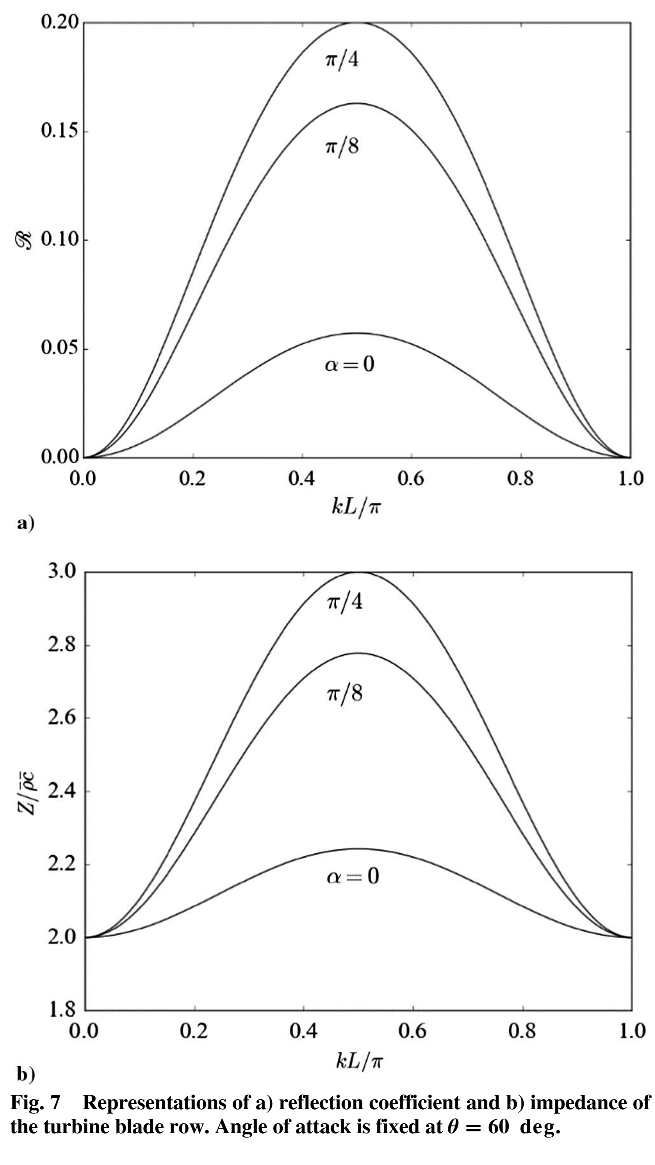

Fig. 7 Representations of a) reflection coefficient and b) impedance of the turbine blade row. Angle of attack is fixed at $\theta = 60$ deg.

rule of thumb. It must not, however, be regarded as a rigorous quantitative criterion because the waves incident on the turbine blade row are not perfectly planar, and because multiple wavelengths are likely to be represented in the acoustic field. Furthermore, it should be emphasized that these impedance values correspond to the case of negligible mean flow, in which the effects of vorticity and entropy waves are not considered.

To incorporate this impedance boundary condition into the acoustic model, the local incidence angle of waves at the boundary must be related to the acoustic velocities via $\tan\alpha = \hat{u}_y/\hat{u}_x$.

III. Results and Discussion

A. Preburner

The overall length of the single preburner is 0.637 m, and its maximum diameter (that of the mixing chamber) is 0.294 m. Additional dimensions are shown in Ref. [2]. Figure 8 shows the acoustic pressure and velocity distributions on a longitudinal cross section of the preburner. The corresponding eigenfrequencies are given in Table 3. The outlet boundary condition is treated as acoustically open to reflect the fact that there is no obstruction at this plane between the preburner and the turbine hub.

B. Assembly of Preburners and Turbine Inlet Hub

For the composite preburner–turbine inlet assembly, several boundary conditions are considered for the turbine inlet annulus: open, closed, and blade row impedance conditions, as discussed previously. Figure 9 shows the acoustic pressure and velocity distributions on a longitudinal cross section of the assembly. The corresponding surface pressure distributions are presented in Fig. 10. Table 4 lists the eigenvalues for all boundary conditions. Because the pressure distributions do not change appreciably for different boundary conditions, they are only presented once.

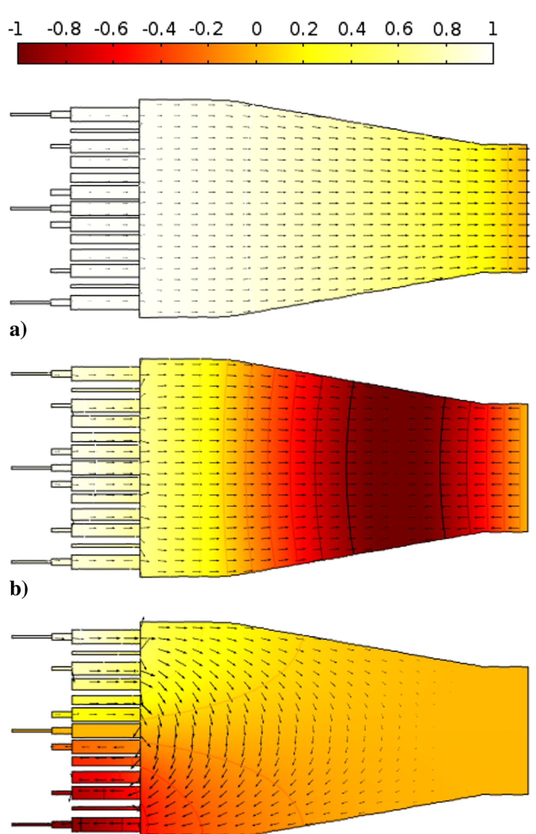

Fig. 8 Acoustic pressure and velocity on longitudinal preburner cross section: a) bulk mode, b) 1L mode, and c) 1T mode.

Table 3 Eigenfrequencies (in hertz) of preburner for acoustically open outlet condition

Mode	Eigenfrequency
Bulk	199
1L	797
1T	995

The lowest mode exhibited by the single preburner geometry is a bulk (Helmholtz) mode in which all pressure and velocity oscillations are in phase everywhere in the chamber and a nodal line is only present at the boundary of the domain. This corresponds to (one-half of) the 2L mode of the composite preburner–turbine inlet assembly, which occurs at approximately the same frequency. Note that Helmholtz-like behavior occurs in each preburner in the composite assembly, but there is no low-pressure region corresponding to the near field of the nodal surface and the frequency does not match. The frequency of the 1T mode identified in the single preburner also agrees exactly with that for the 1T mode identified in the composite preburner–turbine inlet hub assembly. Thus, correspondence between the two geometries is established.

Of particular interest are the decay constants found for the modes of the assembly of the preburners and the turbine inlet hub. Due to its quasi-one-dimensional geometry, the acoustic motions in the system are predominantly longitudinal. One might expect, based on this qualitative observation, that the impedance boundary condition imposed at the turbine inlet annulus would not be "activated" by virtue of its orientation. However, as shown in Fig. 9, the geometry near this region is such that, indeed, there is a component of acoustic velocity normal to the surface, which results in damping of acoustic waves. The frequencies for all the longitudinal modes in the composite assembly are nontrivially changed when the turbine blade row boundary condition is changed; those for the 1L and 3L modes are higher for an acoustically closed boundary than for an open one.

The 1T mode, by contrast, exhibits no damping constant because its oscillations are entirely removed from the turbine inlet annulus, and thus do not experience damping related to this interface. Furthermore, the 1T oscillations on either end of the preburner–turbine assembly are decoupled. In Fig. 9, the oscillations have been manually rotated so that the pressure antinodes may be displayed in a single cut plane. Figure 10d more clearly shows that the spatial orientation of the transverse oscillations in each preburner is independent. This suggests the possibility of unique failure modes associated with transverse oscillations. Were a spinning 1T (or higher) oscillation to develop such that the mode in each preburner spun in a different direction or at a different rate in the same direction, a periodic torque would be developed and would act on the entire assembly. Likewise, if standing 1T oscillations of identical spatial phase in each preburner were to arise, a periodic bending moment would be developed. The determination of which occurrence is more likely would depend on knowledge of the dynamics of spinning waves in the system. Evidence from annular combustors suggests that spinning or standing modes could be preferred depending on factors such as injector swirl, injector spacing, and the equivalence ratio [22].

The 2L mode is revealed to be the most stable with the largest damping coefficient, whereas the 1L mode is the least damped. This trend can be explained by considering the form of the impedance boundary condition. As seen from Fig. 7b, the impedance, and hence the damping, increases with frequency to a maximum at a frequency of approximately 1935 Hz for the present system. Thus, higher longitudinal modes tend to be damped more effectively. The fact that the damping coefficient of the 3L mode is slightly less than that for the 2L mode can be attributed to the slightly shallower average angle of incidence on the turbine blade row exhibited by the oscillations of the 3L mode. In the case in which the boundary is considered acoustically open, the 2L mode is completely suppressed.

No information about the absolute magnitude of the oscillations can be obtained from the present linear analysis. The distribution of acoustic velocity is, however, of interest from a combustion dynamics

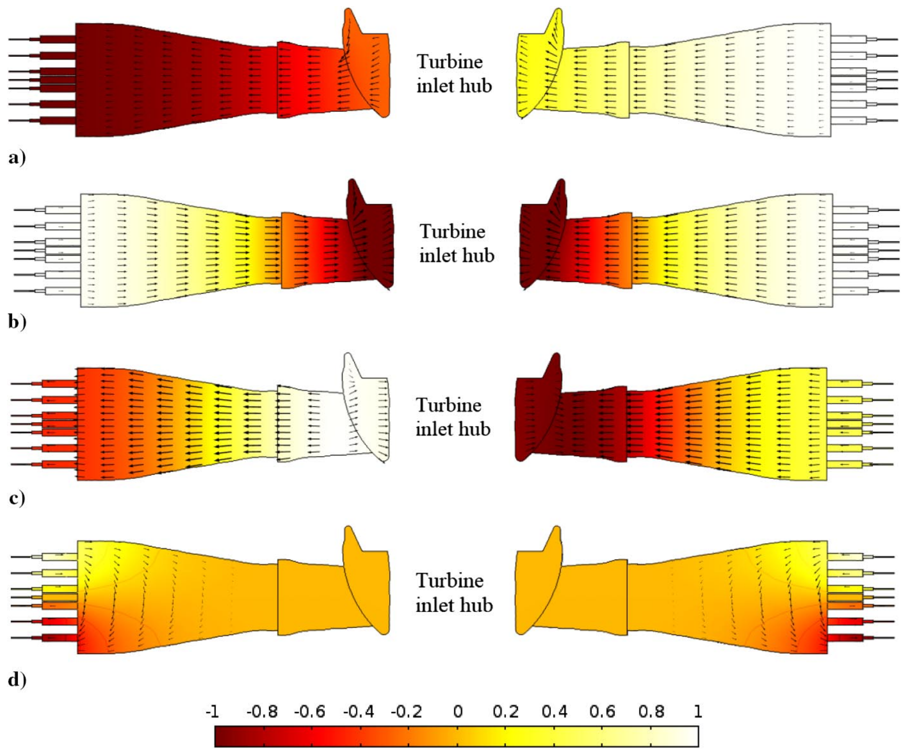

Fig. 9 Acoustic pressure and velocity on inlet hub cross section for modes a) 1L, b) 2L, c) 3L, and d) 1T (reoriented so that nodal surfaces are coplanar).

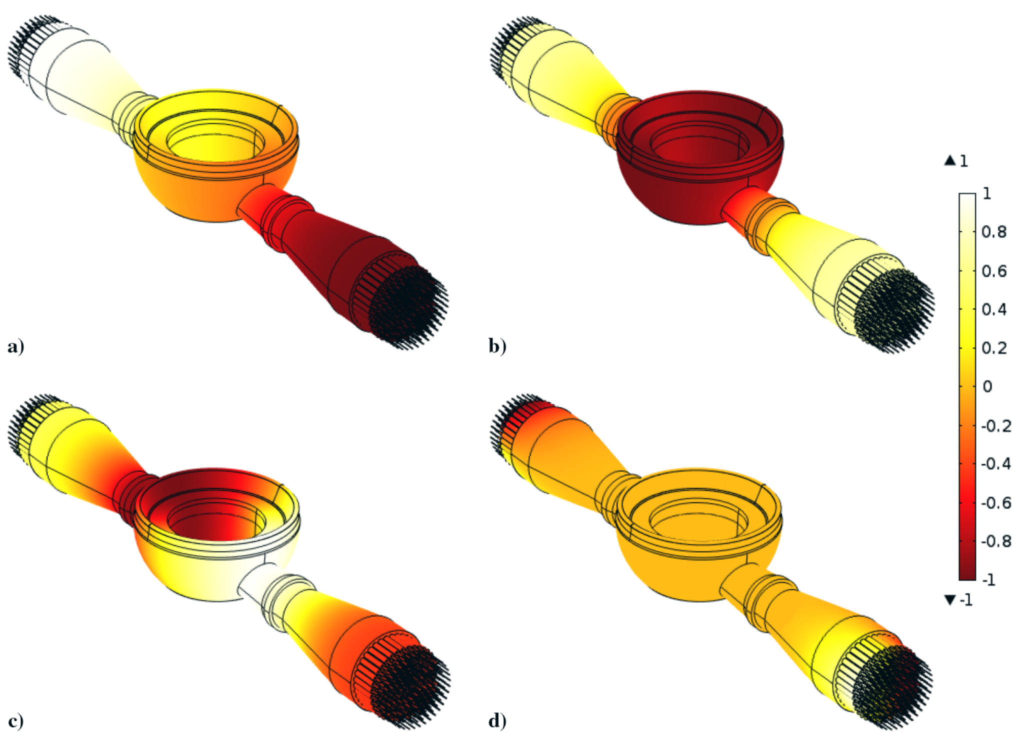

Fig. 10 Surface distributions of acoustic pressure for modes a) 1L, b) 2L, c) 3L, and d) 1T.

Table 4 Eigenfrequencies (in hertz) of preburner–turbine inlet assembly for the indicated boundary condition (BC)

Turbine BC	1L	2L	3L	1T
Closed	113	215.7	423	995
Open	127.5	N/A[a]	541.6	995
Impedance	113 + 2.9i	174.3 + 66.5i	441 + 57.7i	995

[a]N/A denotes "not applicable."

perspective. As indicated by Figs. 9a–9c, the magnitude of the acoustic velocity is lower near the injectors than farther downstream for all longitudinal modes. For the transverse mode, the opposite is the case.

IV. Conclusions

The linear acoustics of an oxygen-rich staged combustion engine preburner assembly similar to that of the RD-170 engine are investigated. The analysis takes into account real fluid properties to accommodate the supercritical fluid state in the preburner. The results show that the mode shapes in the composite assembly of the preburners and the turbine inlet hub are largely invariant with respect to the boundary condition used at the turbine blade row, but the frequencies are noticeably affected. The 2L mode is totally suppressed in the case in which the turbine blade row is considered acoustically open. All longitudinal modes are damped, with the 2L mode possessing the highest decay constant. Both the frequency and mode shape of the 1T mode remain unchanged, regardless of the impedance of the turbine blade row. This phenomenon may be attributed to the fact that the oscillations are confined to the injector regions and do not extend to the impedance surface.

The mode shapes and frequencies for the single preburner geometry agree well with their counterparts for the combined preburner–turbine inlet assembly when an acoustically open boundary condition is applied to the preburner outlet. However, because the domain does not include the turbine inlet plane at which the damping occurs, it is impossible to recover useful stability information from a single preburner model alone. This conclusion mirrors that of previous work [10], which established that a satisfactory stability analysis of the RD-170 main combustion chamber must include a domain encompassing the perforated flow distributor terminating the upstream oxidizer dome.

Additional work is needed to quantify the effects of mean flow, and consequently the effects of turbine rotation rate. Furthermore, a practical stability analysis requires an analysis of the combustion response for the chamber. Such a large-eddy simulation has been performed for the RD-170 main chamber injectors but is still underway for the preburner injectors.

Acknowledgments

This work was sponsored partly by the NASA Marshall Space Flight Center under contract no. NNM12AA41C and partly by the William R. T. Oakes Endowment of the Georgia Institute of Technology.

References

[1] Yang, V., Ku, D. D., Walker, M. L. R., Williams, L., and Leahy, J. C., "Liquid Oxygen/Kerosene Staged Combustion Rocket Engines with Oxidizer-Rich Preburners," NASA TP-2015-218203, 2015.

[2] Yang, V., Ku, D. D., Lioi, C. B., Yeh, S.-T., Leahy, J. C., and Kenny, R. J., "Liquid Oxygen/Kerosene Oxidizer-Rich, Staged Combustion Engine Technology Development," NASA TP-2016-218226, 2016.

[3] Katorgin, B. I., and Chelkis, F. J., "The RD-170, A Different Approach to Launch Vehicle Propulsion," *AIAA/SAE/ASME/ASEE 29th Joint Propulsion Conference and Exhibit*, AIAA Paper 1993-2415, 1993. doi:10.2514/6.1993-2415

[4] Anderson, W. E., and Yang, V., (eds.), *Liquid Rocket Engine Combustion Instability*, Vol. 169, Progress in Astronautics and Aeronautics, AIAA, Washington, D.C., 1995. doi:10.2514/4.866371

[5] Balasubramanian, K., and Sujith, R. I., "Thermoacoustic Instability in a Rijke Tube: Non-Normality and Nonlinearity," *Physics of Fluids*, Vol. 20, No. 4, 2008, Paper 044103. doi:10.1063/1.2895634

[6] Juniper, M. P., "Triggering in the Horizontal Rijke Tube: Non-Normality, Transient Growth and Bypass Transition," *Journal of Fluid Mechanics*, Vol. 667, Jan. 2011, pp. 272–308. doi:10.1017/S0022112010004453

[7] Tamanampudi, G. M. R., and Anderson, W. E., "Development of Combustion Instability Analysis Tool by Incorporating Combustion Response Models," *51st AIAA/SAE/ASEE Joint Propulsion Conference*, AIAA Paper 2015-4165, 2015. doi:10.2514/6.2015-4165

[8] Pieringer, J., Sattelmayer, T., and Fassl, F., "Simulation of Combustion Instabilities in Liquid Rocket Engines with Acoustic Perturbation Equations," *Journal of Propulsion and Power*, Vol. 25, No. 5, 2009, pp. 1020–1031. doi:10.2514/1.38782

[9] Culick, F. E. C., and Yang, V., "Prediction of the Stability of Unsteady Motions in Solid-Propellant Rocket Motors," *Nonsteady Burning and Combustion Stability of Solid Propellants*, Vol. 143, edited by L. De Luca, E. W. Price, and M. Summerfield, AIAA, Washington, D.C., 1992, pp. 719–779.

[10] Lioi, C., Ku, D., and Yang, V., "Linear Acoustic Analysis of Main Combustion Chamber of an Oxidizer-Rich Staged Combustion Engine," *Journal of Propulsion and Power*, advance online publication, 30 July 2018.

[11] Yang, V., "Modeling of Supercritical Vaporization, Mixing, and Combustion Processes in Liquid-Fueled Propulsion Systems," *Proceedings of the Combustion Institute*, Vol. 28, No. 1, 2000, pp. 925–942. doi:10.1016/S0082-0784(00)80299-4

[12] Kaji, S., and Okazaki, T., "Propagation of Sound Waves Through a Blade Row: I. Analysis Based on the Semi-Actuator Disk Theory," *Journal of Sound and Vibration*, Vol. 11, No. 3, 1970, pp. 339–353. doi:10.1016/S0022-460X(70)80038-4

[13] Kaji, S., and Okazaki, T., "Propagation of Sound Waves Through a Blade Row: II. Analysis Based on the Acceleration Potential Method," *Journal of Sound and Vibration*, Vol. 11, No. 3, 1970, pp. 355–375. doi:10.1016/S0022-460X(70)80039-6

[14] Muir, R. S., "The Application of a Semi-Actuator Disk Model to Sound Transmission Calculations in Turbomachinery, Part I: The Single Blade Row," *Journal of Sound and Vibration*, Vol. 54, No. 3, 1977, pp. 393–408. doi:10.1016/0022-460X(77)90448-5

[15] Dowling, A. P., and Mahmoudi, Y., "Combustion Noise," *Proceedings of the Combustion Institute*, Vol. 35, No. 1, 2015, pp. 65–100. doi:10.1016/j.proci.2014.08.016

[16] Cumpsty, N. A., and Marble, F. E., "The Interaction of Entropy Fluctuations with Turbine Blade Rows; A Mechanism of Turbojet Engine Noise," *Proceedings of the Royal Society of London, Series A: Mathematical, Physical and Engineering Sciences*, Vol. 357, No. 1690, 1977, pp. 323–344. doi:10.1098/rspa.1977.0171

[17] Bauerheim, M., Duran, I., Livebardon, T., Wang, G., Moreau, S., and Poinsot, T., "Transmission and Reflection of Acoustic and Entropy Waves Through a Stator–Rotor Stage," *Journal of Sound and Vibration*, Vol. 374, No. 21, 2016, pp. 260–278. doi:10.1016/j.jsv.2016.03.041

[18] Wang, T.-S., "Thermophysics Characterization of Kerosene Combustion," *Journal of Thermophysics and Heat Transfer*, Vol. 15, No. 2, 2001, pp. 140–147. doi:10.2514/2.6602

[19] Meng, H., and Yang, V., "A Unified Treatment of General Fluid Thermodynamics and its Application to a Preconditioning Scheme," *Journal of Computational Physics*, Vol. 189, No. 1, 2003, pp. 277–304. doi:10.1016/S0021-9991(03)00211-0

[20] Lemmon, E. W., Huber, M. L., and McLinden, M. O., "NIST Standard Reference Database 23, Fluid Thermodynamic and Transport Properties REFPROP, User's Guide," National Inst. of Standards and Technology, Gaithersburg, MD, 2013.

[21] Kunz, O., and Wagner, W., "The GERG-2008 Wide-Range Equation of State for Natural Gases and Other Mixtures: An Expansion of GERG-2004," *Journal of Chemical and Engineering Data*, Vol. 57, No. 11, 2012, pp. 3032–3091. doi:10.1021/je300655b

[22] Worth, N. A., and Dawson, J. R., "Modal Dynamics of Self-Excited Azimuthal Instabilities in an Annular Combustion Chamber," *Combustion and Flame*, Vol. 160, No. 11, 2013, pp. 2476–2489. doi:10.1016/j.combustflame.2013.04.031

F. Liu
Associate Editor